JOURNAL OF SPACECRAFT AND ROCKETS
Vol. 45, No. 4, July–August 2008

Forebody Strake Effects on Rocket Aerodynamic Characteristics at High Angles of Attack

William V. Logan,* Roger L. Davis,† and Nesrin Sarigul-Klijn‡
University of California, Davis,
Davis, California 95616
and
Marti Sarigul-Klijn§
AirLaunch, LLC, Kirkland, Washington 98033

DOI: 10.2514/1.35052

The results of a numerical investigation of the forebody strake effects on an air-launched rocket's aerodynamic characteristics at low Mach number and high angles of attack are presented. Forces and moments on a generic rocket that might be used in an air-launch system are predicted using a validated three-dimensional Navier–Stokes code. Asymmetric aerodynamic side forces and yaw moments are observed to occur under certain conditions with 0-deg sideslip, creating conditions of asymmetry. Forces such as these have been observed experimentally on a variety of aerospace vehicles. The effects of forebody strakes on the aerodynamic side forces and yaw moments are presented for 0-deg sideslip angle of attack. In addition, the sources of the aerodynamic characteristics are described. Results show that the forebody strakes reduce side forces and yaw moments by decreasing the magnitude of the streamline vortical interaction and therefore weakening the asymmetric vortical interactions that cause unstable aerodynamic characteristics.

Nomenclature

A	=	cross-sectional area
C_D	=	$[F_x \cos\alpha + F_z \sin\alpha]\cos\beta - F_y \sin\beta$, drag coefficient
C_F	=	$[F_x^2 + F_y^2 + F_z^2]^{1/2}$, force coefficient
C_L	=	$F_x \sin\alpha + F_z \cos\alpha$, lift coefficient
C_l	=	roll moment coefficient about X axis
C_M	=	$[C_l^2 + C_m^2 + C_n^2]^{1/2}$, moment coefficient
C_m	=	pitch moment coefficient about Y axis
C_n	=	yaw moment coefficient about Z axis
C_Y	=	$[F_x \cos\alpha + F_z \sin\alpha]\sin\beta + F_y \cos\beta$, sideslip coefficient
CP	=	C_M/C_F, center of pressure
c	=	speed of sound
d	=	diameter
F_x	=	force coefficient in X direction
F_y	=	force coefficient in Y direction
F_z	=	force coefficient in Z direction
L	=	rocket length
l	=	length of nose cone
M	=	Mach number
ψ	=	$\tan^{-1}(C_{Y/}C_L)$, angle between resultant and normal force

Subscripts

ref	=	reference conditions
∞	=	freestream conditions

I. Introduction

ASYMMETRIC aerodynamic side forces and yaw moments often occur on a variety of aerospace vehicles even though flight conditions are such that no side gusts or sideslip angles are present. Asymmetric forces usually occur at low Mach number and high angle of attack (AOA). The sources of asymmetry have often been traced to the forebody region of the vehicle. Experiments on military fighter aircraft [1], including the F-18 [2–5], F-16 [6,7], and generic fighters [8–10] have previously been performed at low Mach number and high angle-of-attack conditions to quantify side forces and demonstrate various control devices that may be used to remove or reduce the aerodynamic source of asymmetry.

Similar sources of aerodynamic side forces have also been observed experimentally on ogive cylindrical bodies such as rocket nose cones [11–13]. Different control strategies have been used on these bodies to reduce or eliminate the flow asymmetries and corresponding forces and moments. Reviews of various approaches have been given by Malcolm [1], Williams [14], and Ericsson and Reding [15]. Active unsteady bleed was demonstrated by Bernhardt and Williams [16] for the control of asymmetric vortices on a forebody configuration at a 45 deg angle of attack. Two modes of instability were identified in their investigation as the source of the flow asymmetries. These modes include a bistable global mode that was insensitive to proportional control and a convective-type mode in which proportional control reduced side forces. The mode type of instability was a function of the angle of attack and the Reynolds number. Most passive stability control investigations found in open literature have focused on using fore- and/or aftbody strakes to reduce or eliminate side forces due to vortex asymmetries and breakdown. Passive and active control of the asymmetric vortices off a forebody using a miniature nose-tip strake were described by Ming and Gu [17]. It was demonstrated in their investigation that bistable (global) asymmetric flow could be changed from one stable mode to the other through the use of a turbulence-generating rod upstream of the forebody. They also demonstrated that the side forces and flow asymmetries could be reduced to zero by using a miniature nose-tip

Presented as Paper 0549 at the 45th AIAA Aerospace Sciences Meeting and Exhibit, Reno, NV, 8–11 January 2007; received 9 October 2007; revision received 1 February 2008; accepted for publication 5 March 2008.

*Mechanical and Aeronautical Engineering Department. Student Member AIAA.

†Professor, Mechanical and Aeronautical Engineering Department; davisrl@ucdavis.edu. Associate Fellow AIAA.

‡Professor and Leader of Space Engineering Research and Graduate Program (SpaceED), Mechanical and Aeronautical Engineering Department; nsarigulklijn@ucdavis.edu. Associate Fellow AIAA.

§Chief Engineer of Airdrop. Member AIAA.

strake that swung around the centerline at a high frequency. Aftbody strakes and forebody fins were investigated by Lopera et al. [18] for the passive control of flow asymmetries of a blunt-nose projectile at high angles of attack. Their investigation showed that both leading-edge and aftbody strakes were effective in controlling side forces. The use of forebody strakes and a small geometrical perturbation were numerically investigated by Kistan et al. [19] for the passive control of asymmetric vortices generated at the nose of a blunt-ogive forebody. In their investigation, four strakes with 0.06–1.2d height and 0.4–1.0d chord were placed 0.5–1.7d from the nose tip at 45 deg angles to help control the asymmetric vortices that existed at an angle of attack of 40 deg.

This paper presents the results of a numerical investigation on the effects of forebody strakes on an air-launched rocket at low Mach number, high angles of attack, and 0 deg sideslip. At these conditions, aerodynamic instabilities can occur as a result of side forces generated from asymmetry in the flow vortical structure on the downwind side of the rocket. The effect of forebody strakes on these side forces and yaw moments is of particular interest in the current investigation. The predicted effects of engine thrust on the aerodynamic characteristics and flow/load asymmetries for the rocket without strakes were previously described [20]. Validation of the steady-flow Reynolds-averaged Navier–Stokes code against experimental data for a nose cone configuration [21] under the same Mach number and various high angle-of-attack conditions was performed [20] to demonstrate the capability to accurately predict these flows and regions of asymmetric aerodynamic side forces and yaw moments.

The results in this paper were derived based on the assumption of steady-state or time-independent flow. The current investigation does not consider the aerodynamic effects while accelerating from free fall. Consideration of dynamic effects would entail an unsteady simulation with time-varying flight conditions requiring significant computer resources that were not feasible in the current investigation. For the same reason, detached-eddy and large-eddy simulations of the flow at fixed freestream conditions were not considered. The present study focuses on predicting the forces and flow physics at the instants just before engine ignition with "steady" Reynolds-averaged simulations. The current investigation focuses on flow conditions with zero sideslip. Further investigation is required to determine the effects of the current forebody strake configurations in the presence of sideslip.

II. Numerical Approach

The current approach is to use a 3-D Reynolds-averaged Navier–Stokes procedure, OVERFLOW [22], developed at the NASA Ames Research Center, to determine the steady pressure loads on the rocket at various angles of attack and freestream conditions. Steady-flow simulations of the rocket with forebody strakes were performed at low-speed freestream Mach number, a 60 deg angle of attack, and 0 deg sideslip to the oncoming flow.

Some previous numerical investigations [23] of rocket aerodynamic pressure loads found in the open literature have been performed using computationally efficient Euler (inviscid) solution procedures. Because the Reynolds number of the flow is very high (of the order of 5×10^7), the assumption of inviscid flow might be reasonable and justifiable if flow separation is not present or the location of flow separation is fixed. However, flow separation does occur off various positions on the aft surfaces of the rocket, especially at moderate to high angles of attack, significantly altering the pressure loads on the rocket and introducing asymmetric side forces and yaw moments. To eliminate any errors due to neglecting the effects of separation and viscous shear (because the separation location is unknown), the Reynolds-averaged Navier–Stokes equations were solved in the current approach, and all viscous flow layers and wakes were resolved. By using a Reynolds-averaged Navier–Stokes solution procedure [12,19,24–26], the drag due to viscous shear as well as the effects of the separated flow on the pressure drag can be determined. Use of detached-eddy or large-eddy simulations to investigate the vortex asymmetries and breakdown was beyond the scope of the current investigation due to the lack of computational resources and time.

The OVERFLOW code solves the Reynolds-averaged Navier–Stokes equations using second-order accurate spatial central differencing and the Spalart–Allmaras turbulence model. The Spalart–Allmaras model [27] was chosen to model the turbulence because of its wide use for strongly inviscid/viscous interacting flows [28] and computational efficiency. A blended second- and fourth-difference dissipation scheme is used to achieve monotonically smooth solutions, to capture shocks, and to eliminate numerical instabilities. A fully implicit lower/upper symmetric Gauss–Seidel (LU-SGS) relaxation procedure is used to integrate the equations in time. Typical solutions of the rocket in the current investigation converged in 20,000–75,000 iterations depending on the freestream conditions (primarily Mach number). As the Mach number decreased, the region of separated flow on the downstream surfaces of the rocket increased in size. At very low Mach numbers, the region of separated flow became unsteady, and flow shedding was encountered. An adiabatic, no-slip boundary condition was held at all solid surfaces. The wall spacing (distance of first grid point away from the wall) was held at approximately 2×10^{-4} mm. The steady loading on the rocket was determined by considering a fixed upstream Mach number, Reynolds number, angle of attack, and sideslip angle.

III. OVERFLOW Validation

An experimental investigation was previously conducted at the NASA Ames Research Center to measure side forces on forebodies at high angles of attack and Mach numbers [21]. The trade study proved that, for various nose cones, separation occurs at the nose rather than the aftbody of the rocket. A single nose cone of similar geometry to the air-launched rocket, the NB2 nose cone, was chosen from the NASA investigation and modeled in OVERFLOW to validate the software [20]. The NB2 nose cone has a length-to-diameter ratio l/d of 2.84 with a 20 deg nose cone angle. The Reynolds number and Mach number in the wind-tunnel experiments were 1×10^6 and 0.25, respectively. Under these conditions, the flow over the NB2 nose cone separated before the end of the cone. Each nose cone in the wind-tunnel investigation produced similar results. NASA engineers concluded from these experiments that separation off the rocket at high angles of attack occurs off the nose rather than off the body.

This conclusion is consistent with the findings from the current numerical investigation. The OVERFLOW predictions [20] showed that the overall trends and absolute levels of side forces were in good agreement with the experimental data, with a region of aerodynamic instability (defined as a Mach number region in which asymmetric side forces occur due to fluid dynamic instability under flight conditions at 0 deg sideslip) existing at angles of attack between 40 and 80 deg, with the largest asymmetry at 75 deg angle of attack. The differences between the predicted and the experimental side-force coefficients varied at most by a factor of 0.2 for all angles of attack between 0 and 90 deg. The good comparison between predicted side forces and identification of the origin of the side forces with the NB2 nose cone configuration gave credence to the use of OVERFLOW for rocket predictions of the same phenomena. Details of the OVERFLOW validation for high angle-of-attack flow over the nose cone are given in [20].

IV. Computational Model

In this section, a description of the grid generation process is provided to describe how the rocket model was generated in Chimera Grid Tools. Similar to the process used for the NB2 nose cone, the surface grid for the rocket was generated by concatenating and equidistributing points. The grid is uniformly spaced in the circumferential direction, stretched in the axial direction to achieve the curvature of the rocket's geometry, and clustered in the radial direction to capture the viscous flow. The rocket surface grid resolution is $121 \times 195 \times 93$ (circumferential x axial x radial) grid

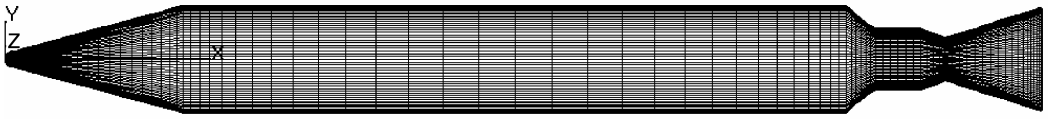

Fig. 1 Rocket surface computational grid.

points (see Fig. 1 and Table 1). For details of the rocket's geometry, refer to [29].

A. Forebody Strake Geometry and Surface Grid

The forebody strakes were modeled with simple rectangular sides and a top cap. Two overlapping grids were used to mesh the strake to the top cap and rocket. Grid spacing between the strakes, rocket, and top caps was kept consistent. Four grids in total were generated for each strake (see Tables 2 and 3).

Two forebody strake geometries were designed for this investigation. The 0.04 (nondimensional value based on the height of the strake divided by the reference radius of the rocket) cropped forebody strakes were designed with a width of 3.18 mm and a height of 44.5 mm, placed in the middle position or half the length of the rocket nose cone (see Table 2). The second 0.15 cropped forebody strakes examined the effect of increasing the size of the forebody strakes. The 0.15 cropped forebody strakes were designed with a width and height of 158.8 mm, also placed in the middle position of the rocket nose cone (see Table 3). Smaller surface grid spacing was required for the 0.04 cropped forebody strakes due to its smaller width in comparison to the 0.15 strakes. Both strakes had a length of 1.73 m or one-half the rocket nose cone length. Both the 0.04 and 0.15 cropped forebody strakes were analyzed at three orientations including 0, 45, and −45 deg relative to the rocket's centerline (see Fig. 2).

Table 1 Zone grid dimensions of rocket

Zone	Name	Circumferential	Axial	Radial
1	Nose cap	24	24	93
2	Rocket	121	195	93
3	Tail cap	22	22	93
4	Strake 1	36	149	88
5	Strake 1 top cap	9	57	88
6	Strake 1 bottom overlap	14	149	75
7	Strake 1 top overlap	13	129	88
8	Strake 2	36	149	88
9	Strake 2 top cap	9	57	88
10	Strake 2 bottom overlap	14	149	75
11	Strake 2 top overlap	13	129	88

Table 2 Zone grid dimensions of 0.04 cropped forebody strakes

Zone	Name	Circumferential	Axial	Radial
12	Forebody strake 1	177	38	79
13	Top cap 1	85	5	79
14	Rocket strake overlap 1	177	12	79
15	Strake top-cap overlap 1	177	10	79
16	Forebody strake 2	177	38	79
17	Top cap 2	85	5	79
18	Rocket strake overlap 2	177	12	79
19	Strake top-cap overlap 2	177	10	79

Table 3 Zone grid dimensions of 0.15 cropped forebody strakes

Zone	Name	Circumferential	Axial	Radial
12	Forebody strake 1	93	13	84
13	Top cap 1	41	7	84
14	Rocket strake overlap 1	93	13	84
15	Strake top-cap overlap 1	93	9	84
16	Forebody strake 2	93	13	84
17	Top cap 2	41	7	84
18	Rocket strake overlap 2	93	13	84
19	Strake top-cap overlap 2	93	9	84

B. Rocket Volume Grid

A volume grid for each zone was constructed in Chimera Grid Tools by specifying the boundary conditions, number of points, distance into the far field, initial and end spacing, and smoothing parameters. An average wall spacing of 2×10^{-4} mm was used for each zone of the multigrid rocket, corresponding to an average Reynolds number of approximately 7.93×10^{6} (value based on reference diameter). The volume grid was extended into the far field a distance of one rocket length in all directions. Beyond one rocket length, OVERFLOW generated off-body grids [22] extending three rocket lengths into the far field amounting to a total far-field distance of four rocket lengths. Staying consistent with the surface grid generation, a stretching ratio of 1.2 was used. For each zone, two volume grids were created. The first grid represented the boundary layer extending 10 points with an initial and end spacing of 2×10^{-4} mm. The second grid was stretched a distance of one rocket length in the radial direction from an initial spacing of 2×10^{-4} mm to an end spacing of 1.68 m. The rocket grid was periodic in the circumferential direction along the 360-deg single radial plane. The grid spacing near the outer boundaries of the strake entities was consistent to those of the local rocket grid.

The rocket computational grid size including the far-field grids for strake-off conditions consists of 11 zones amounting to 3,789,030 grid points (see Table 1). The 19-zone multigrid rocket equipped with the 0.04 cropped forebody strakes consists of 7,795,342 grid points (see Tables 1 and 2). The 19-zone multigrid rocket, equipped with the 0.15 cropped forebody strakes, requires 4,879,218 grid points (see Tables 1 and 3). These computational grid dimensions and wall spacing were consistent with previous numerical simulations and grid-refinement investigations at the same Reynolds number in which the solution was grid independent. In addition, the grid dimensions and wall spacing were consistent with the computational grid used in the OVERFLOW validation solution.

C. Flow Solution and Boundary Conditions

A fixed Courant–Friedrichs–Lewy (CFL) number (nondimensionalized by the length and freestream speed of sound) of 5.0 was used for the rocket without forebody strakes. Typical convergence was 20,000–50,000 iterations, or 72–120 h, using eight CPUs of a Linux cluster. Simulations with forebody strakes called for a fixed CFL number as low as 2.0. Typical convergence with forebody strakes was 20,000–75,000 iterations, or 72–160 h, using eight CPUs of a Linux cluster. Decreasing the time-step size increased the computational time by increasing the number of iterations to reach convergence. A viscous adiabatic wall was used for all solid surfaces in all simulations. The rocket held a circumferential periodic boundary condition along the single radial plane.

V. Results

A series of subsonic flow cases were run in OVERFLOW to analyze the effects that forebody strakes have on the rocket's aerodynamic characteristics at high angles of attack. This analysis was done by predicting the side forces and yaw moments about the rocket for varying Mach numbers at an altitude of 2438.4 m and a 60 deg angle of attack. Mach numbers were varied by 0.05 from 0.05 to 0.60. Side- and yaw-force instabilities (regions in which

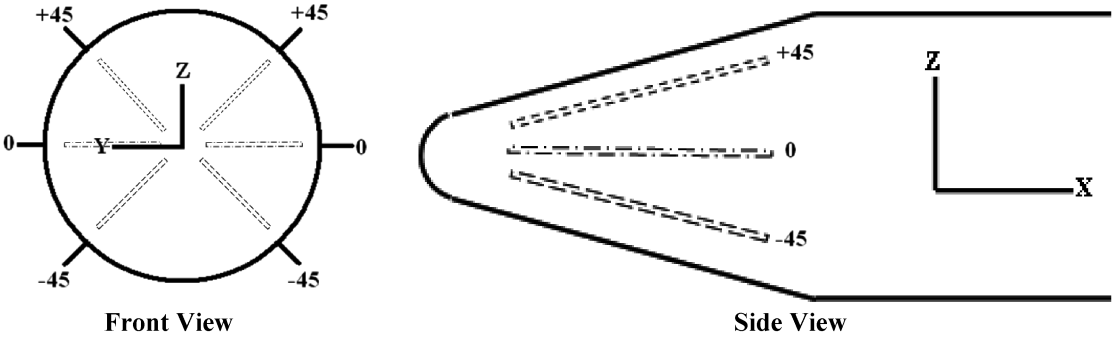

Fig. 2 Orientations of forebody strakes in simulation (front and side views of rocket).

asymmetric side forces and yaw moments due to fluid dynamic instability were predicted under flight conditions at 0 deg sideslip) were determined for the rocket without forebody strakes in two Mach number regions: 0.08–0.15 and 0.40–0.50 [20]. The first velocity flow regime (Mach 0.8–0.15) represents the flow just after launch from the aircraft. The second velocity flow regime (Mach 0.40–0.50) is representative of the flow just before engine ignition. In these flow regions, figures of the surface pressure, velocity, vorticity, and streamlines were generated to determine what triggers these existing asymmetric side forces and yaw moments. It was determined that the greatest point of asymmetry within each of the two Mach number regions exists at Mach 0.10 and 0.40 [20]. The rocket was then analyzed at each point of asymmetry with forebody strakes at three orientations (0, 45, and −45 deg) relative to the centerline to investigate the forebody strakes effect on the aerodynamic characteristics. The current investigation analyzed these effects at a 0 deg sideslip angle of attack. Further investigation is required to determine the effects of the forebody strake configurations in the presence of sideslip.

A. No Forebody Strakes

Details of the OVERFLOW simulation results of the rocket at a 60 deg angle of attack without forebody strakes were shown as part of a separate investigation of engine thrust effects on the side forces and yaw moments [20]. Some results without forebody strakes are shown here to make comparison with the forebody strake results straightforward.

The nondimensional forces in the X, Y, and Z directions were illustrated for a 60 deg angle of attack vs the Mach number for the rocket without forebody strakes [20]. The largest force coefficient in the Y direction in the low Mach number region of instability was 1.207 (2436.1 N) occurring at a Mach number of 0.10. The maximum force coefficient in the Y direction for the smaller high Mach number region of instability equaled 0.135 (4353.6 N) occurring at a Mach number of 0.40.

Asymmetric aerodynamic characteristics were determined based on the magnitude of the moments about the leading-edge point of the rocket. The center of gravity of the rocket is located 11.68 m in the axial direction from the nose. The nondimensional moments (roll, pitch, and yaw) were shown for 60 deg angle of attack vs the Mach number for cases without forebody strakes [20]. The yaw moment, acting around the Z axis, was analyzed at both Mach number regions determined from the force coefficient in the Y direction. The largest force in the Y direction occurred at Mach 0.10, where the yaw moment coefficient equaled 0.586 (23, 751.0 N · m). At the higher Mach number region of instability, the largest yaw moment coefficient of 0.104 (67, 580.2 N · m) occurred at a Mach number of 0.40, as suggested by the force coefficient in the Y direction.

Streamlines were analyzed to investigate the unstable vortex structures that cause the asymmetric aerodynamic side forces and yaw moments on the rocket [20]. At the low Mach number region, a large force coefficient in the Y direction occurred at a Mach number of 0.10, resulting in a large yaw moment. According to NASA Langley Research Center's report [21] and the nose cone study [20], large forces in the Y direction caused asymmetric separation of the streamlines off the nose and an asymmetric vortex breakdown. The streamlines validated NASA's conclusion, separating asymmetrically off the nose, creating an asymmetric after-body vortex interaction.

This asymmetric vortex behavior is caused by the incoming freestream flow expanding around the nose of the rocket, causing the velocity to increase to a maximum. The pressure, in contrast to the velocity, decreases to a minimum point. As the flow expands beyond the nose and the relative minimum pressure point, the pressure begins to increase, creating an adverse pressure gradient. The flow due to this adverse pressure gradient initially separates symmetrically off the nose with a core vortex that revolves clockwise on the left side and counterclockwise on the right side (as viewed in the $+X$ direction). This opposite-direction rotation leads to an interaction between the left-side and right-side vortices. A strong vortex interaction resulting from counter-rotating vortices causes asymmetric flow on the aftbody of the rocket, leading to an asymmetric adverse pressure gradient on the nose. The asymmetric adverse pressure gradient causes the streamlines to separate asymmetrically and an asymmetric vortex interaction. The asymmetric vortex interaction would likely manifest itself as vortex (Strouhal) shedding in an unsteady simulation. In the current steady-flow simulations, the asymmetric vortex interaction converges to a fixed, stable state. Aerodynamic side- and yaw-force instabilities are a result of an asymmetric vortex interaction often referred to as a vortex breakdown.

The alternating asymmetric vortex behavior on the upper surface of the rocket originates from the boundary layers underneath and to each side of the rocket. As the flow separates on the aft side of the rocket, the vorticity reaches a critical strength, moves circumferentially in the direction of rotation, and then sheds from the surface. The vortices on each side of the rocket alternate with this pattern along the length of the rocket.

A vortex breakdown is precisely what occurs at Mach 0.10 for the rocket without forebody strakes. As the simulation converges, the streamlines separate asymmetrically, causing the side forces and yaw moments at Mach 0.10. A force coefficient in the positive Y direction of 1.207 (2436.1 N) acts at the rocket's center of pressure, 10.02 m in the axial direction, relative to the rocket's center of gravity 11.68 m in the axial direction (see Table 4). The rocket experiences a yaw moment in the positive direction of 0.586 (23, 751.0 N · m), which, in a transient solution, would cause the nose of the rocket from the front view to rotate to the left about the center of gravity. A time-independent Ψ rotation angle (see Nomenclature) was calculated to introduce a measure of sideslip or yaw angle of attack that the rocket would experience in a transient solution. The rocket at Mach 0.10, due to the side and yaw asymmetries, would encounter a 24.4-deg, time-independent rotation angle.

At the high Mach number point of instability (Mach 0.40), the rocket experiences smaller-scale asymmetries in comparison to those at Mach 0.10. At steady-state equilibrium, a side force of 0.135 (4353.6 N) acting at the center of pressure 8.33 m from the nose causes a yaw moment of 0.104 (67, 580.2 N · m) (see Table 4). The yaw moment leads to a resulting time-independent rotation angle of 3.14 deg, a more realistic and controllable instability. Further details of the results at Mach 0.40 can be found in [20].

Table 4 Force and moment summary

	No forebody strakes (fbs)	0.04 cropped fbs at 0 deg	0.04 cropped fbs at +45 deg	0.04 cropped fbs at −45 deg	0.15 cropped fbs at 0 deg	0.15 cropped fbs at +45 deg	0.15 cropped fbs at +45 deg
M, no.				**0.10**			
F_y, N	2,436.10	165.20	−375.80	92.00	156.20	302.60	413.50
CP, m	10.02	7.85	9.55	8.36	7.91	9.06	8.93
C_n, N · m	23,751.00	2,110.90	−6, 150.00	−2, 959.00	−420.30	925.90	2,131.70
Ψ, deg	24.40	−3.70	−4.86	0.82	1.40	3.15	3.70
M, no.				**0.40**			
F_y, N	4,353.60	1,322.10	−2, 108.00	4,594.00	294.30	5,965.00	−2, 790.00
CP, m	8.33	8.15	8.74	8.80	7.93	8.25	8.47
C_n, N · m	67,580.20	10,580.10	54,283.00	52,806.00	−2272.00	98,107.00	−36, 807.00
Ψ, deg	3.14	0.90	−1.47	3.09	0.18	4.03	−1.87

B. Forebody Strakes

The forebody strake effects on the air-launched rocket are presented in this section. The 0.04 cropped forebody strakes were analyzed at both Mach number points of aerodynamic instability to determine whether forebody strakes would alter the side- and yaw-force asymmetries. The side forces and yaw moments were analyzed at three orientations (see Fig. 2) relative to the centerline on the rocket nose.

The forebody strakes placed at 0 or 180 deg apart on the Y axis were most successful at reducing the aerodynamic side force and yaw moment asymmetries to 0 at a 0 deg sideslip angle of attack (see Fig. 3). At Mach 0.10, the rocket experiences a force coefficient in the Y direction of 0.082 (165.16 N) and a yaw moment coefficient of 0.052 (2110.9 N · m), leading to a time-independent Ψ rotation angle of −3.70 deg. These results show reduced side-force and moment magnitudes compared with the rocket without strakes, in which a force in the Y direction of 1.207 (2436.1 N) and a yaw moment of 0.586 (23, 751.0 N · m) lead to a time-independent Ψ rotation angle of 24.4 deg. At Mach 0.40, the 0.04 cropped forebody strakes reduced the force in the Y direction from 0.135 (4,353.6 N) to 0.041 (1322.1 N) and the yaw moment from 0.104 (67, 580.2 N · m) to 0.016 (10, 580.1 N · m). The time-independent Ψ rotation angle was reduced from 3.14 to 0.90 deg. The strakes also moved the center of pressure forward from 10.02 to 7.85 m from the nose. Increasing the distance between the center of gravity and the center of pressure, or rather static margin, increases the static stability and controllability of the rocket during flight (see Fig. 3 and Table 4).

The 0.04 cropped forebody strakes were also investigated at 45 and −45 deg relative to the centerline on the rocket nose. The forebody strakes at 45 deg decreased the time-independent Ψ rotation angle from 24.43 to −4.86 deg at Mach 0.10 and 3.14 to −1.47 deg at Mach 0.40. The forebody strakes at −45 deg reduced the time-independent Ψ rotation angle to 0.82 and 3.09 deg, respectively. The forebody strakes placed at 0 deg relative to the centerline were more successful at reducing the aerodynamic asymmetries on the rocket compared with the rocket without strakes (see Fig. 4 and Table 4).

The rocket equipped with the 0.04 cropped forebody strakes at the 0 deg position experiences relatively zero side- and yaw-force asymmetries, as shown in Fig. 3. Based on the results and the previous analysis for the rocket without forebody strakes, the strakes should reduce the vortex interaction between the left-side and right-side streamlines. The streamlines and pressure contours shown in Figs. 5 and 6 illustrate that the 0.04 cropped forebody strakes reduce the vortex interaction and corresponding surface pressure, as well as generate symmetric pressure contours.

The rocket equipped with the 0.04 cropped forebody strakes at the 45 and −45 deg orientations experiences larger side- and yaw-force asymmetries compared with the 0 deg position (see Fig. 4). The streamlines with forebody strakes at the 45 and −45 deg positions should verify these results with larger more asymmetric vortex

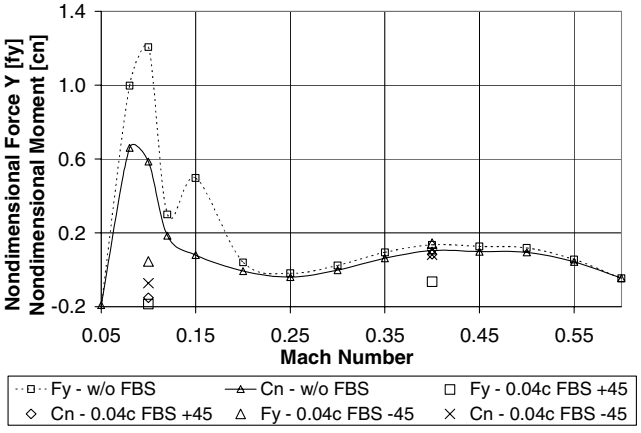

Fig. 4 Nondimensional forces and moments vs Mach number: 0.04*c* forebody strakes at 45/ − 45 deg.

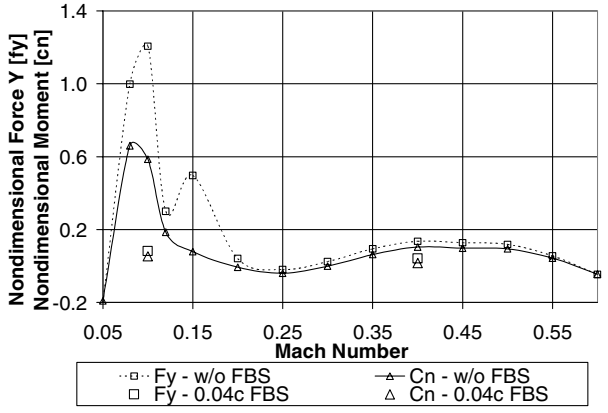

Fig. 3 Nondimensional forces and moments vs Mach number: 0.04*c* forebody strakes at 0 deg.

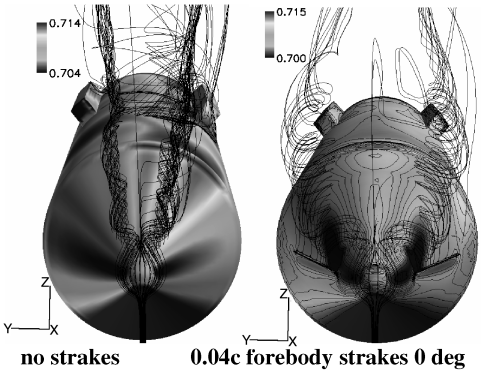

Fig. 5 Mach 0.10 streamlines in *X* direction and surface pressure contours.

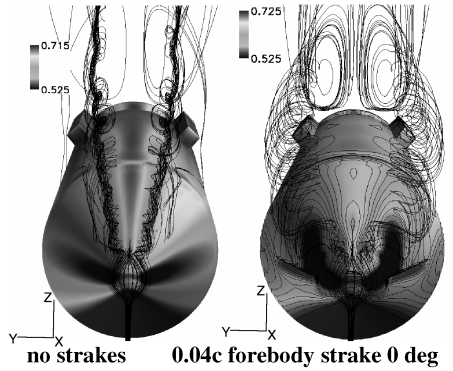

Fig. 6 Mach 0.40 streamlines in *X* direction and surface pressure contours.

interactions between the left-side and right-side vortices. The slight asymmetries in the vortex interactions complimented with the larger surface pressure and more asymmetric pressure contours (see Figs. 7 and 8) reiterate that the 0 deg strake position reduces the vortex interaction and corresponding side- and yaw-force asymmetries at a 0 deg sideslip angle of attack more effectively than at the 45 and −45 deg orientations.

The cause of the reduction in the aerodynamic side- and yaw-force asymmetries by the forebody strake at the 0 deg orientation was investigated. Forebody strakes alter the vortex interaction by reducing the velocity and increasing the relative pressure of the freestream flow. This interaction reduces the adverse pressure gradient, causing the streamlines to separate symmetrically at a different position on the nose. The corresponding vortices from the nose are weaker, reducing the vortex interaction. The forebody strakes alter the vortex interaction by changing the position of separation and weakening the magnitude of the vortices.

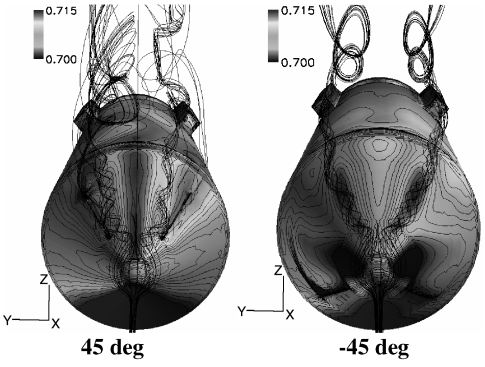

Fig. 7 Mach 0.10 streamlines in *X* direction and surface pressure contours: 0.04*c* forebody strakes.

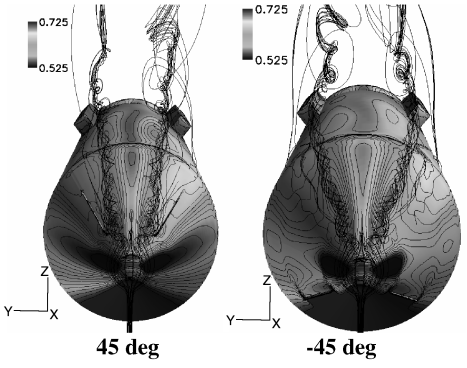

Fig. 8 Mach 0.40 streamlines in *X* direction and surface pressure contours: 0.04*c* forebody strakes.

Results show that the larger 0.15 cropped forebody strakes were more effective in reducing the aerodynamic side force and yaw moment asymmetries to 0 compared with the 0.04 cropped forebody strakes. The 0.15 cropped strake placed at the 0 deg orientation reduced the side-force coefficient in the *Y* direction compared with 156.2 N at Mach 0.10 and 294.3 N at Mach 0.40. The yaw moment was reduced −420.3 and $-22,720.0$ N · m at Mach 0.10 and 0.40, respectively. The time-independent Ψ rotation angles were reduced at Mach 0.10 and 0.40 to 1.40 and 0.18 deg, respectively, compared with −3.70 and 0.90 deg for the 0.04 cropped forebody strakes (refer to Table 4). The vortex cores (see Figs. 9 and 10) confirm these results, as the vortices are tighter with greater spin compared with the vortices for the 0.04 cropped strakes.

Though the 0.15 cropped forebody strakes at the 0 deg position were more effective in reducing the asymmetries (the greatest deviation at Mach 0.40), the larger strakes also increased the drag. The larger 0.15 cropped forebody strakes increased the drag compared with the rocket without strakes by an average of 7.9% at Mach 0.10 and 30.9% at Mach 0.40. This drag increase is in comparison to the 0.04 cropped forebody strakes, which decreased the drag at Mach 0.10 by 17.6% while increasing by 18.6% at Mach 0.40. This trend leads to a tradeoff between aerodynamic stability and efficiency. As the size of the strake increases, the stability of the rocket improves; however, the aerodynamic efficiency of the rocket decreases.

The 0.15 cropped forebody strakes positioned at 45 and −45 deg relative to the centerline were slightly more effective than the 0.04 cropped counterparts, except at Mach 0.40, where the 0.15 cropped forebody strakes at the 45 deg position performed worse. The forebody strakes at 45 deg decreased the time-independent Ψ rotation angles to −3.15 deg at Mach 0.10 and 4.03 deg at Mach 0.40 (see Table 4). The forebody strakes at −45 deg reduced the time-independent Ψ rotation angles to 3.70 and −1.87 deg,

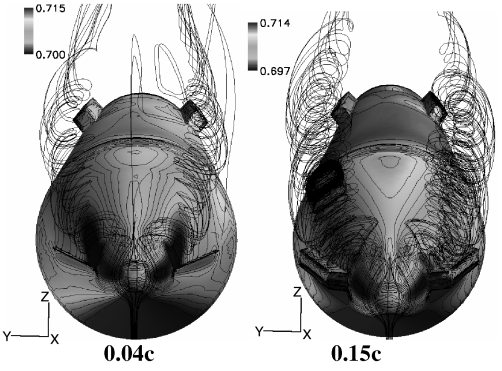

Fig. 9 Mach 0.10 streamlines in *X* direction and surface pressure contours: strakes at 0 deg.

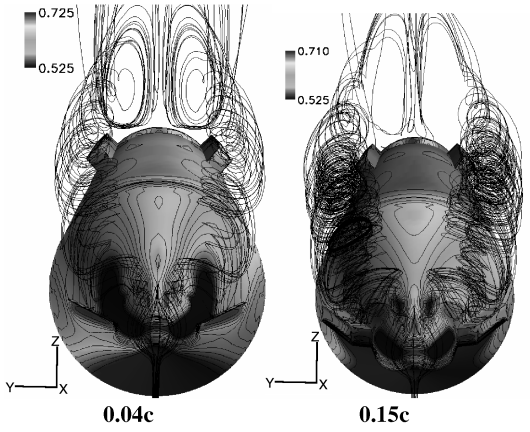

Fig. 10 Mach 0.40 streamlines in *X* direction and surface pressure contours: strakes at 0 deg.

respectively (see Table 4). Though the larger 0.15 cropped strakes effectively reduced the aerodynamic asymmetries, the drag coefficient of the rocket increased.

VI. Conclusions

Results from a numerical investigation of the forebody strake effects on the aerodynamic characteristics of an air-launched rocket at high angle of attack have been presented. Regions of asymmetry due to side forces and yaw moments are predicted to occur on the air-launched rocket in certain Mach number regimes. These asymmetries have been found to result from strong vortical interactions, which cause asymmetries in the flow structure and surface pressure. Forebody strakes are determined to significantly reduce side- and yaw-force asymmetries for high angle-of-attack flow by inducing symmetric separation off the nose and thereby decreasing the magnitude of the streamline vortical interaction. The 0.04 cropped forebody strakes at the 0 deg strake position on the rocket effectively reduced the aerodynamic side force and yaw moment asymmetries without severely increasing the drag.

References

[1] Malcolm, G. N., "Forebody Vortex Control: A Progress Review," AIAA Paper 93-3540-CP, 1993.

[2] Lanser, W. R., and Murri, D. G., "Wind Tunnel Measurements on a Full-Scale F/A-18 with Forebody Slot Blowing or Forebody Strakes," AIAA Paper 93-1018, 1993.

[3] Ng, T. T., and Malcolm, G. N., "Aerodynamic Control Using Forebody Blowing and Suction," AIAA Paper 91-0619, 1991.

[4] Ng, T. T., Suarez, C. J., and Malcolm, G. N., "Forebody Vortex Control Using Slot Blowing," AIAA Paper 91-3254, 1991.

[5] Ng, T. T., and Malcolm, G. N., "Aerodynamic Control Using Forebody Strakes," AIAA Paper 91-0618, 1991.

[6] LeMay, S. P., Sewall, W. G., and Henderson, J. F., "Forebody Vortex Flow Control on the F-16C Using Tangential Slot and Jet Nozzle Blowing," AIAA Paper 92-0019, 1992.

[7] Suarez, C. J., Malcolm, G. N., and Ng, T. T., "Forebody Vortex Control with Miniature Rotatable Nose-Boom Strakes," AIAA Paper 92-0022, 1992.

[8] Malcolm, G. N., Ng, T. T., Lewis, L. C., and Murri, D. G., "Development of Non-Conventional Control Methods for High Angle of Attack Flight Using Vortex Manipulation," AIAA Paper 89-2192, 1989.

[9] Malcolm, G. N., and Ng, T. T., "Forebody Vortex Manipulation for Aerodynamic Control of Aircraft at High Angles of Attack," SAE Paper 892220, 1989.

[10] Skow, A. M., Moore, W. A., and Lorincz, D. J., *Forebody Vortex Blowing: A Novel Concept to Enhance the Departure/Spin Recovery Characteristics of Fighter Aircraft*, CP-262, AGARD, May 1979.

[11] Ericsson, L. E., "Thoughts on Conical Flow Asymmetry," *AIAA Journal*, Vol. 31, No. 9, Sept. 1993, pp. 1563–1568.

[12] Degani, D., and Schiff, L. B., "Numerical Simulation of the Effect of Spatial Disturbances on Vortex Asymmetry," *AIAA Journal*, Vol. 29, No. 3, March 1991, pp.344–352.

[13] Ng, Y. T., Lim, T. T., Luo, S. C., and Lua, K. B., "Effects of Probe Interference on Side Force of an Inclined Ogive Cylinder," *AIAA Journal*, Vol. 42, No. 2, 2003, pp. 420–423.

[14] Williams, D., "A Review of Forebody Vortex Control Scenarios," AIAA Paper 97-1967, 1997.

[15] Ericsson, L. E., and Reding, J. P., "Alleviation of Vortex-Induced Asymmetric Loads," *Journal of Spacecraft and Rockets*, Vol. 17, No. 6, 1980, pp. 546–553.

[16] Bernhardt, J. E., and Williams, D. R., "Proportional Control of Asymmetric Forebody Vortices," *AIAA Journal*, Vol. 36, No. 11, Nov. 1998, pp. 2087–2093.

[17] Ming, X., and Gu, Y., "An Innovative Control Technique for Slender Bodies at High Angle of Attack," AIAA Paper 2006-3688, June 2006.

[18] Lopera, J., Ng, T. T., Mehul, P. P., and Vasudevan, S., "Yaw Control of a Blunt-Nose Projectile at High Angles of Attack Using Strakes," AIAA Paper 2007-671, Jan. 2007.

[19] Kistan, P., Gobey, S. G., and Law, C., "Effect of Forebody Strakes on a CFD-Created Asymmetric Flowfield," AIAA Paper 2006-3843, June 2006.

[20] Logan, W. V., Davis, R. L., Sarigul-Klijn, N., and Sarigul-Klijn, M., "Engine Thrust Effects on Air-Launched Rocket Aerodynamic Characteristics at High Angle of Attack," *Journal of Spacecraft and Rockets*, Vol. 44, No. 2, March–April 2007, pp. 338–346.

[21] Keener, Earl R. Chapmann, Gary, T., Cohen, L., and Taleghani, J., "Side Forces on Forebodies at High Angles of Attack and Mach number from 0.1 to 0.7: Two Tangent Ogives, Paraboloid and Cone," NASA TM X-3438, 1977.

[22] Buning, P. G., Chan, W., Renze, K. J., Sondak, D., Chiu, I. T., Slotnick, J. P., Gomez, R., and Jespersen, D., "Overflow User's Manual," NASA Ames Research Center, Moffett Field, CA, 1995 [available online], http://freespeech.sourceforge.net/doc/user-manual/.

[23] Priolo, F. J., and Wardlaw, A. B., Jr., "Euler Space-Marching Computations with Cross flow Separation for Missile-Type Bodies," AIAA Paper 1990-616, 1990.

[24] Bulbeck, C. J., Morgan, J., and Fairlie, B. D., "RANS Computations of High-Incidence Missile Flow Using Hybrid Meshes," AIAA Paper 2000-4209, 2000.

[25] Josyula, E., "Computational Study of High-Angle-of-Attack Missile Flows using Two-Equation Turbulence Models," AIAA Paper 1998-525, 1998.

[26] Birch, T. J., Wrisdale, I. E., and Prince, S. A., "CFD Predictions of Missile Flowfields," AIAA Paper 2000-4211, 2000.

[27] Spalart, P. R., and Allmaras, S. R., "A One-Equation Turbulence Model for Aerodynamic Flows," AIAA Paper 92-0439, Jan. 1992.

[28] Sinha, K., Mahesh, K., and Candler, G., "Modeling the Effect of Shock Unsteadiness in Shock/Turbulent Boundary-Layer Interactions," *AIAA Journal*, Vol. 43, No. 3, March 2005, pp. 586–594.

[29] Dornheim, M. A., "Air Drops Dummy Rocket for DARPA's Falcon," *Aviation Week and Space Technology*, Oct. 2005 [available online], http://www.aviationweek.com/aw/generic/story_generic.jsp?channel=awst&id=news/102405p1.xml.

M. Costello
Associate Editor